RESEARCH ARTICLE

Selective Targeting and Accumulation of Aluminum in Tissues of C57BL/6J Mice Fed Aluminum Sulfate Activates a Pro-inflammatory NF-kB-microRNA-146a Signaling Program

Pogue AI[1]*, Zhao Y[2,3]*, Jaber V[2], Percy ME[4], Cong L[5], Lukiw WJ[1,5,6,7]

[1]Alchem Biotek Research, Toronto ON, Canada.
[2]LSU Neuroscience Center, Louisiana State University Health Sciences Center New Orleans, New Orleans LA, USA.
[3]Department of Anatomy and Cell Biology, Louisiana State University Health Sciences Center New Orleans, New Orleans LA, USA.
[4]Department of Neurogenetics, University of Toronto, Toronto ON, Canada.
[5]Department of Neurology, Shengjing Hospital, China Medical University, 36 No.3 Street, Heping District, Shenyang, Liaoning Province, China.
[6]Department of Ophthalmology, Louisiana State University Health Sciences Center New Orleans, New Orleans LA, USA.
[7]Department of Neurology, Louisiana State University Health Sciences Center New Orleans, New Orleans LA, USA.

Abstract

Several independent laboratories using different murine-strains have reported **(i)** that the supplementation of mouse-diets and/or drinking water with aluminum significantly enhances neuro-inflammatory signaling in specific brain-tissue compartments when compared to age-matched controls; and **(ii)** that these aluminum-induced changes resemble an inflammatory-neuropathology characteristic of Alzheimer's-disease (AD) brain. In this communication using an analytical time-course of 1, 3 and 5 months in aluminum-fed C57BL/6J mice, here for the first time, we quantify: **(i)** in which of the 25 mouse-tissues analyzed is aluminum targeting/accumulating; and **(ii)** the degree-of-induction of NF-kB and the pro-inflammatory microRNA-146a (miRNA-146a) in regions of the brain that displayed the highest aluminum-accumulation. Methodologies included naturally-aging, wild-type C57BL/6J female murine-models, DNA-expression arrays, ELISA, electrothermal atomic-absorption spectrophotometry (ETAAS) and bioinformatics analysis. The five most significant findings were: **(i)** of the 25 murine-tissues examined all tissues accumulated aluminum to various degrees; **(ii)** aluminum-accumulation was age-related and appeared to be highest in the brain/retina, breast-tissues and ovaries; **(iii)** most tissues ceased rapid aluminum-accumulation after approximately 1 month; **(iv)** certain tissues such as the brain/retina, breast-tissue and ovaries continued to accumulate aluminum up to 5 months (the longest time-point studied); and **(v)** aluminum accumulation was directly-associated with a significant up-regulation of NF-kB and the pro-inflammatory miRNA-146a in the same tissues. Taken together the results indicate that in aluminum-fed C57BL/6J murine-models aluminum not only selectively accumulates in nervous and reproductive tissues but also significantly induces a pro-inflammatory gene signaling program in anatomical regions which normally exhibit high-metabolic rates and high-levels in the readout of genetic-information.

Keywords: Neurotoxin; Aluminum sulfate; Cortex; Cerebellum; Hippocampus; Retina and microRNA-146a

Abbreviations: AD: Alzheimer's disease, ANOVA: Analysis of variance, BMA: Bone marrow, BRN: Whole brain, BRS: Breast, C57BL/6J: Common strain of laboratory mouse, CER: Cerebellum, CTX: Cortex, ETAAS: Electrothermal atomic absorption spectroscopy, HRT: Heart, HIP: Hippocampus, MiRNA: Micro RNA, NF-Kb: Nuclear factor for kappa B (a pro-inflammatory transcription factor), OVY: Ovary, PIT: Pituitary, RNA Pol II: RNA polymerase type II, RET: Retina, ROS: Reactive oxygen species

Introduction

Consisting of 8.8% (w/v) of the earth's crust, aluminum is a ubiquitous metallic neurotoxin and genotoxin to which humans are heavily exposed throughout their lives. The intake of an average of 10 mg Al/day (range 10–1000 mg Al/day) occurs chiefly via the ingestion of food, water, medicine and inhalation [1-5]. Fortunately, the low solubility of aluminum at biological pH and highly evolved epithelial-, and endothelial-

cell-based gastrointestinal (GI) and blood-brain barriers (BBB) prevent this ubiquitous metallotoxin from accessing human biological compartments. Importantly, aluminum that does gain entry into the central nervous system (CNS) in animal models has been shown to induce NF-kB and microRNA-146a-mediated inflammatory and neuroimmune pathogenic gene expression patterns that closely emulate many aspects of CNS pathology and progressive memory dysfunction that are highly characteristic of neurodegenerative disorders which include Alzheimer's disease (AD) [1,6-18].

The current experimental studies were undertaken to advance our understanding of the targeting, tissue distribution and accumulation of aluminum in 25 tissues from wild type control C57BL/6J mice at 1, 3 and 5 months after feeding these mice with aluminum-sulfate in their daily food and drinking water. Control animals were fed magnesium sulfate to normalize for sulfate intake and were analyzed in parallel. Using ELISA-, DNA array-based analyses the levels of the pro-inflammatory transcription factor NF-kB and the NF-kB-regulated inflammatory miRNA-146a were quantified in samples exhibiting the highest aluminum accumulation. Importantly, activation of NF-kB-miRNA-146a regulated signaling pathways is a potent precursor to the establishment of pro-inflammatory gene expression programs in the mammalian CNS with downstream, pathogenic consequences [12-14,17-23].

Materials and Methods

C57BL/6J animals

C57BL/6J control animals purchased from a commercial rodent research supplier (http://jaxmice.jax.org/ jaxnotes/507/507r. html; Jackson Laboratories, Bar Harbor, MA, USA) were housed and raised at the LSU animal breeding and holding facility as previously described [6,7]. There were 2 test groups - a magnesium sulfate fed-and-watered 'control' test group and an aluminum-sulfate fed-and-watered test group. Typically 36 female animals per test group were randomized and selected to receive either standard rodent chow (meal-ground pellets; Standard Laboratory rodent diet 5001; http://www.labdiet. com/cs/groups/lolweb/@labdiet/documents/web_content/ mdrf/mdi4/~edisp/ducm04 _028021.pdf; LabDiet St. Louis MO, USA), or a diet enriched in Al (as sulfate; commonly used as food additive and water purification agent; http://www. generalchemical.com/assets/pdf/Dry_Alum_ Food_Grade_ PDS.pdf; 100 mg Al/kg diet; LD50 for aluminum sulfate in mice ~980 mg Al/kg). Control animals received drinking water containing 0.2 mg/L aluminum (https://www.wqa. org/Portals/0/Technical/Technical%20Fact%20Sheets/ 2014 Aluminum.pdf; http://www.who.int/water_sanitation_health/ publications/aluminium/en/) and aluminum-treated animals received aluminum-supplemented water (2.0 mg/L aluminum). The aluminum content of both food and water are realistic in the consumer environment for daily human exposure; both food and water were provided *ad libitum* from birth. C57BL/6J mice stopped weaning and started eating either standard rodent chow or a diet enriched in Al at about 1 month of age (time

'0'); at 0, 1, 3 and 5 months animals were sacrificed, tissues and organs were harvested under RNAse-free clean conditions and were subjected to Zeeman-type ETAAS trace metal analysis for aluminum (detection limit ~0.1 ug/L).

Murine tissues, chemicals and reagents, protein extraction and quality control

Analytical chemicals and reagents used in these experiments were obtained from standard commercial suppliers; all chemicals and reagents were used in accordance with the manufacturer's specifications and without any additional purification. Age-matched magnesium sulfate control and aluminum-sulfate-treated C57BL/6J tissues at 0, 1, 3 and 5 months of age were analyzed for aluminum from both control and aluminum-fed animals; total tissue DNA, RNA and protein were isolated using TRIzol reagent as previously described by our group [21-23]; DNA, RNA and protein samples were archived for further downstream analysis. Protein concentrations were determined using a dotMETRIC microassay as previously described (sensitivity 0.3 ng protein/ ml; Invitrogen, Carlsbad, CA, USA; Chemicon-Millipore, Billerica, Massachusetts, USA) [21-23; 24-31].

Aluminum analysis and ETAAS

Sample Preparation: Up to 0.5 gm of individual tissues (wet weight) were dissected free of connective tissue and vasculature and washed in ultrapure water (18 megohm, Millipore or Puriss 95305, Milli-Q water; Fluka; Tracepur® product 1.00473 EMD Merck-Millipore Bellerica MA, USA; aluminum content <1 ppb), were next 'dry' ashed in platinum crucibles, taken up in concentrated ultrapure HNO_3 (OmniTrace UltraTM Nitric acid NX0408, EMD Merck-Millipore, or ULTREX II Ultrapure Reagent, J.T.Baker/VWR Radnor PA, USA; aluminum content ~20 ppt) and subjected to ETAAS as previously described by our laboratory and others [18-29]. Some murine tissues were pooled to achieve enough tissue mass to make up to a 0.5 gm wet weight. Parallel sets of samples were also analyzed using the 'wet'-digestion method of Trap et al (1978) and Van der Voet (1985) as modified by van Ginkel et al., (1990) [18-20]. In the later method 0.5 gm samples of tissue in disposable polypropylene or Teflon tubes were incubated 24 hr at 45℃ in 0.8 mL concentrated ultrapure nitric acid and 0.2 ml concentrated ultrapure sulfuric acid (ULTREX II Ultrapure Reagent, J.T.Baker/VWR Radnor PA, USA; aluminum content <50 ppt) in a dedicated thermomixer/ extractor device (Eppendorf Incorporated, Hauppauge NY, USA); the temperature was raised to 70℃ for 3 hrs and then 105℃ resulting in a clear yellow solution, diluted up to 3.0 ml with ultrapure water and subjected to trace metal analysis.

Analytical Parameters, controls and independent analysis: trace metal analysis was performed in duplicate or triplicate on 20 uL samples using electrothermal atomic absorption spectrophotometry (ETAAS); PE5000PC system, Zeeman-type, Perkin-Elmer, Waltham MA, USA) equipped with an PE 18-position automated sampler and an IBM/AT-supported analysis package for trace metal analysis, as previously described by our group and others [18,19,25-29]. Briefly,

the ETAAS device hollow-cathode lamp was operated at 15 mA; atomic absorption for aluminum was measured at 309.3 nm with a spectral band width of 0.7 nm; the purge gas was Argon at 300 ml/min; gas flow was interrupted at atomization; typically the dry cycle was 130ºC, 10 sec ramp, 5 sec hold; char cycle 1500ºC, 18 sec ramp with a 6 sec hold; the atomize cycle was 2700ºC with a 0 sec ramp and a 6 sec hold, although other programs were used with quantitatively similar results; aluminum concentrations in the digest were determined using the standard-addition method. In the later a 10 mg/L aluminum aqueous solution was prepared from ultrapure reagents; aqueous standard solutions of 0, 10, 20 and 50 ug/L were prepared; typically a 250 uL sample of digest was mixed with an equal volume of standard solution prior to analysis in duplicate [19-23; SJ Karlik, G Van der Voet, P Zatta; personal communications). Additional details of the aluminum determination procedure using ETAAS are given in **Figure 1** and **Supplementary File 1**. Random murine tissue samples were also checked for aluminum content and confirmed independently using a Perkin Elmer ETAAS device at the Department of Physiology, Medical Sciences Building, University of Toronto. Some brain samples were in addition analyzed using experimental X-ray fluorescence (XRF) spectroscopy at the Advanced Photon Source (APS), Argonne National Laboratory, University of Chicago.

ELISA analysis for the NF-kB (p65) subunit

ELISA analysis for the pro-inflammatory NF-kB transcription factor' were performed using an NF-kB p65 polyclonal antibody [PA1-186; Invitrogen-Thermo Fisher Scientific, Waltham MA, USA] and a control protein marker β-actin (3598–100; Sigma-Aldrich Chemical Company, St. Louis, Missouri, USA) using methodologies previously described by our laboratory [18-20]. The abundance of the NF-kB (p65) subunit in aluminum-treated versus control samples for 25 murine tissues is shown in bar graph format in figures.

Statistical analysis, data interpretation and integrated bioinformatics analysis

For ETAAS data, ELISA and DNA array analysis all statistical procedures were analyzed using (p, ANOVA) a two-way factorial analysis of variance using algorithms and procedures in the SAS language (Statistical Analysis Institute, Cary, NC, USA) and as previously described [21-23]. In the results p-values of less than 0.05 (ANOVA) were considered to be statistically significant. All aluminum, NF-kB and miRNA-146a data were collected and analyzed using Excel 2016 (Office 365) algorithms (Microsoft Corporation, Redmond WA, USA); all figures were generated using Adobe Illustrator CC 2015 and Photoshop CC version14.0 (Adobe Corporation, San Jose CA, USA). All statistical procedures for ELISA were analyzed using a two-way factorial analysis of variance (p, ANOVA) using programs and procedures in the SAS language (Statistical Analysis Institute, Cary, NC, USA) and as previously described [29-31]. Only p-values of less than 0.05 (ANOVA) were considered to be statistically significant.

Figures were generated using Excel 2008 (Microsoft Corporation, Redmond WA), Adobe Illustrator CS3 ver 11.0 and Photoshop CS2 ver 9.0.2 (Adobe, San Jose CA).

Results

Figure 1 displays in bar graph format the extent of aluminum accumulation in 25 tissues of wild-type C57BL/6J female murine-models fed aluminum (as sulfate) for 1, 3 and 5 months. A general trend is seen in that certain tissues (such as the BMA – bone marrow, WBL – white blood cells, LYN – lymph node, THY – thymus, HRT – heart, SKM – skeletal muscle, SMM – smooth muscle, KID – kidney, LIV – liver, SPL – spleen, STO – stomach, BLA – bladder, and PIT – pituitary) accumulate modest levels of aluminum while other tissues such as BRN – (whole) brain, CTX – cortex, CER – cerebellum, HIP – hippocampus, RET – retina, BRS – breast, and OVY – ovary show a more robust aluminum uptake, especially at 5 months, the longest time-point studied in these experiments. In these experiments C57BL/6J murine tissue values ranged from about 25-450 ng aluminum per gm wet weight of tissue for the 5 month time-point analyzed (**Figure 1**); **Figure 2** shows NF-kB levels in the 7 tissues that accumulated the most aluminum at 5 months including whole brain (BRN), cortex (CTX), cerebellum (CER), hippocampus (HIP), retina (RET), breast (BRS) and ovary (OVY) compared to two tissues – thymus (THY) and heart (HRT) that did not display high levels of aluminum accumulation.

Expression of miRNA-146a is known to be driven by the activation of 3 canonical NF-kB binding sites in the miRNA-146a proximal promoter by NF-kB-DNA binding **(Figure 3A)**; hence any tissue that displayed a high level of induction of NF-kB also showed a parallel induction of miRNA-146a expression, often considered first step in the initiation of inflammatory signaling. A robust example of this is the stress-activated increases in NF-kB and miRNA-146a expression in human brain primary cells and AD coupled to the observed miRNA-146a-induced decrease in the expression of the key anti-inflammatory complement factor H (CFH) [22,23,31]. Indeed independent analysis using miRNA microfluidic array-based analysis and global miRNA profiling showed a significant increase in miRNA-146a expression in these same tissues (**Figure 3B**); these results are depicted in bar graph format in (**Figure 3C**).

Discussion and Conclusions

It remains an intriguing question why aluminum should selectively accumulate in CNS and reproductive tissues when compared to other tissue types. It is well understood that the high charge density of aluminum (3+) has an exceptionally high affinity for biological phosphates, and the highest densities of phosphate groups are located in the polyphosphate backbones of nucleic acids including DNA and RNA in all of their forms as well as in the adenine mono-, di- and tri-phosphates of the nucleus and cytoplasm [1,4,5,32-37]. Cells of tissues with high metabolic rates such as those encountered in the brain, retina and reproductive tissues appear to generally have a more open
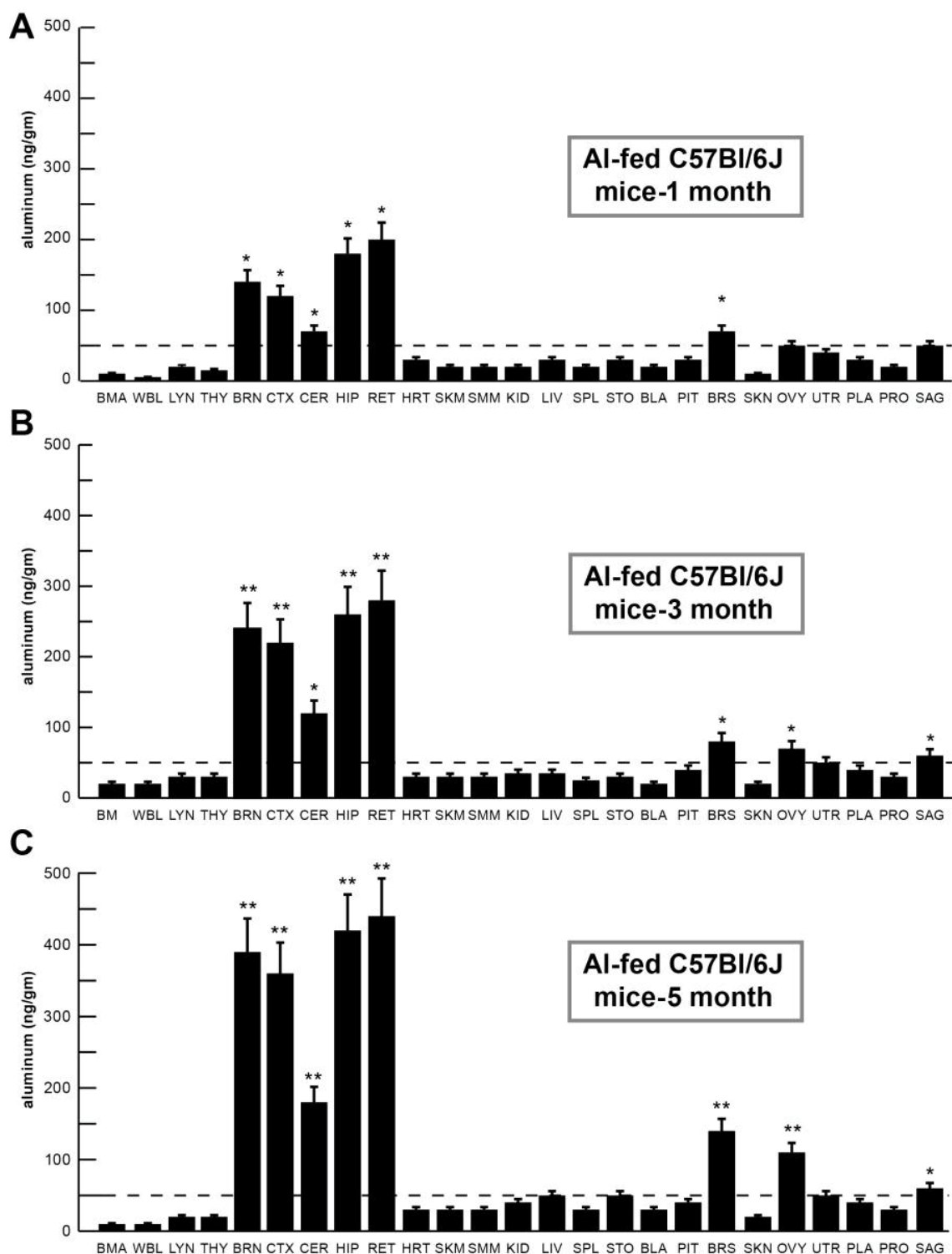
3

Figure 1: Time course of aluminum content of tissues isolated from 1, 3 and 5 moth old C57BL/6J mice receiving aluminum sulfate in their food and drinking water; 'wet digestion' method shown here; tissues analyzed: BMA – bone marrow, WBL – white blood cells, LYN – lymph node, THY – thymus, BRN – (whole) brain, CTX – cortex, CER – cerebellum, HIP – hippocampus, RET – retina, HRT – heart, SKM – skeletal muscle, SMM – smooth muscle, KID – kidney, LIV – liver, SPL – spleen, STO – stomach, BLA – bladder, PIT – pituitary, BRS – breast, SKN – skin, OVY –ovary, UTR – uterus, PLA –placenta, PRO – pancreas, SAG – salivary gland; note (i) aluminum uptake in all tissues analyzed and (ii) selective accumulation of aluminum in brain and retinal tissues (BRN, CTX, CER, HIP, RET) and reproductive tissues (BRS, OVY; see text); some tissues were pooled from several animals to achieve sufficient tissue mass for elemental analysis; for RET analysis either whole (pooled) retina or whole murine globes were used (~25 mg per single globe); BRN, BRS, OVY and RET (either whole retina or whole globes) exhibited the largest increases in aluminum at the 5 month period; both the 'dry ashing' and the 'wet digestion' method (see text) gave quantitatively similar results and aluminum accumulation patterns; N = 3 to 5; *p< 0.05; **p<0.01 (ANOVA); a horizontal dashed line at 50.0 is shown for ease of comparison.
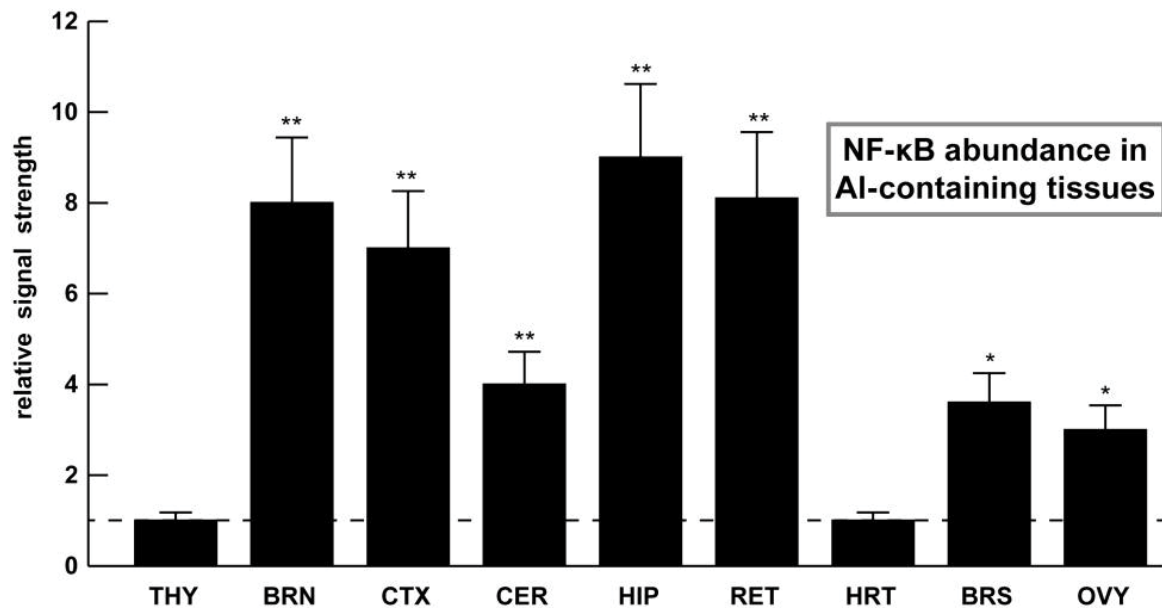
Figure 2: Up-regulated NF-kB signaling in select tissues of C57BL/6J mice fed aluminum sulfate for 5 months; certain murine tissues accumulate aluminum (see text and Figure 1); of the 25 tissues studied aluminum accumulated the most in the whole brain (BRN), hippocampus (HIP) and retina (RET) followed by breast tissues (BRS) and ovaries (OVY); in these same tissues NF-kB was found to be up-regulated in parallel; in these experiments the largest increase amongst all tissues in aluminum-fed C57BL/6J mice was a 9-fold increase in NF-kB abundance between the thymus (THY) and hippocampus (HIP); a dashed horizontal line is included at 1.0 for ease of comparison; N= 3 to 5 samples; *$p<0.05$, **$p<0.01$ (ANOVA).

or 'euchromatic' distribution of genetic material within the nucleus which may make them more available for attraction of trivalent aluminum species with polyphosphate via strong electrostatic interactions [1,4,21,29]. We therefore speculate that perhaps tissue types with a more open, 'euchromatic' or 'transcriptionally permissive' distribution of genetic material may make these cell types especially prone to interaction with aluminum. Interestingly, it has been recently suggested that dietary effects may be linked to the selective uptake, targeting and accumulation of aluminum into different cellular and nuclear compartments [28,33,38-46]. Put another way this may mean that the composition of the diet may affect the extent of aluminum, or other neurotoxin, uptake into susceptible tissues.

After 1 month of aluminum-sulfate feeding to wild-type C57BL/6J female murine-models there is a modest accumulation of aluminum in most of the 25 tissues studied albeit to various degrees. After 5 months of aluminum-sulfate feeding to these C57BL/6J mice there is as much as a 3.0-fold increase in the amount of aluminum accumulation in the CNS tissues studied [compare RET (retina), HIP (hippocampus), CER (cerebellum) and CTX (cortex) in **Figure 1**]. These are aluminum accumulations of, respectively, 2.2-, 2.3-, 2.6-, and 3.0-fold over controls. The fact that aluminum accumulates to some extent in all of the 25 tissues studied suggests that aluminum feeding may be capable of inducing aluminum-ROS-NF-kB-miRNA-146a-mediated pro-signaling pathways in all tissues which receive exposure, although again, to various degrees. A pathological aluminum entry system into the brain and CNS, mediated by the endothelial cells that line the cerebral vasculature and microvasculature has been described – this system directs blood supply to selective anatomical targets throughout the CNS with downstream pathogenic and pro-inflammatory consequences [29]. This study further suggests that nervous (brain, retina) and reproductive tissues (ovary) with high metabolic rates may be especially susceptible to aluminum accumulation and hence aluminum's neurotoxic effects (**Figure 1**).

Within these same tissues that aluminum accumulates is observed, in parallel, a very significant increase in the abundance of NF-kB as detected by ELISA analysis **(Figure 2).** It is noteworthy to point out that all tissues derived from aluminum-fed C57BL/6J female murine-models showed varying degrees of NF-kB up-regulation and hence potential activation of the aluminum-ROS-NF-kB-miRNA-146a-mediated pro-signaling circuits. It is not known in tissues with low aluminum uptake and low levels of NF-kB increase whether this may be responsible for a type of 'slow and smoldering', self-sustaining and 'chronic' inflammation as has been described for the time course of AD neuropathology [34-38]. Activation of the pre-formed pro-inflammatory transcription factor (TF) NF-kB by reactive oxygen species (ROS), ROS–mediated phosphorylation of NF-kB-inhibitor IkB, release of the activated NF-kB TF dimer, and subsequent NF-kB-DNA binding to gene promoters are important key components of the induction of inflammatory signaling in AD and other types of progressive, age-related inflammatory neurodegenerations [30-35]. It has been previously demonstrated that aluminum salts are strong inducers of ROS, and hence activators of NF-kB leading to binding of NF-kB to DNA receptors in gene promoters, and increased transcription from down-stream
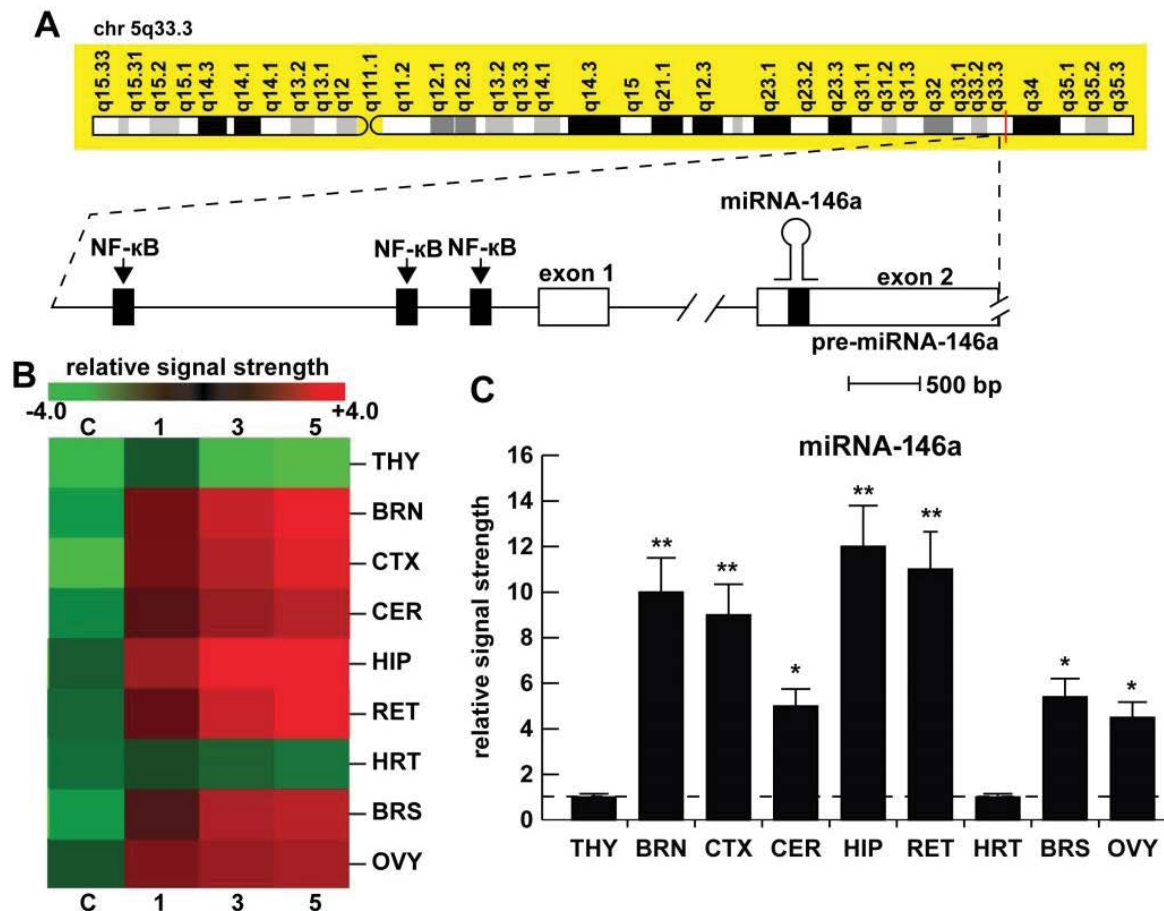
Figure 3: Up-regulation of a pro-inflammatory NF-kB-miRNA-146a circuit in tissues of C57BL/6J mice fed aluminum sulfate; (A) the single copy gene encoding miRNA-146a encoded at human chromosome 5 (at chr5q33.3; overlaid in yellow; not drawn to scale; upper panel) and the promoter structure of the miRNA-146a gene indicates position of 3 canonical NF-kB-DNA binding sites in the proximal promoter (lower panel); all 3 NF-kB-DNA binding sites have been shown to be functional indicating that NF-kB up-regulation efficiently drives miRNA-146a expression [21-23]; (B) miRNA-array-based color-coded cluster analysis of miRNA-146a up-regulation in 9 tissues in which aluminum accumulates in C57BL/6J mice fed aluminum sulfate in their diets and drinking water for 1 3, and 5 months versus control animals (c); control diets were supplemented with magnesium sulfate to control/normalize for sulfate (magnesium is an overwhelmingly abundant divalent cation in biological tissues); (C) color-coded cluster analysis converted to bar graph format for data in (B) indicating significant miRNA-146a up-regulation in brain (BRN), cortex (CTX), cerebellum (CER), hippocampus (HIP), retina (RET) breast (BRS) and ovary (OVY) but not thymus (THY) or heart (HRT) tissues; N = 3 to 5 samples for each analysis; *$p< 0.05$; **$p<0.01$ (ANOVA); in (C) a dashed horizontal line at 1.0 is included for ease of comparison.

genes whether they be protein-encoding- or microRNA-type genetic elements [35-39]. Up-regulation in the expression of the pro-inflammatory microRNA miRNA-146a is a known consequence of increased NF-kB binding to a triplet of canonical NF-kB recognition sites in the upstream promoter of miRNA-146a gene located on the long arm of chromosome 5 at chr5q33.3 (**Figure 3**) [23,28,31]. As a consequence of increased miRNA-146a there are post-transcriptional gene regulatory programs put into play that direct pro-inflammatory and pathogenic gene signaling, and ultimately brain cell decline and apoptotic cell death.

Lastly, this investigation provides at least five novel and significant findings: **(i)** that of all of the 25 murine-tissues analyzed in these experiments each accumulated aluminum to various extent; **(ii)** that the accumulation of aluminum into tissues was time-dependent and attained the highest levels in

nervous tissues of the CNS and in reproduction-associated tissues including ovarian tissues; **(iii)** that after aluminum feeding of animals the majority of tissues ceased to rapidly accumulate aluminum after approximately 1 month; **(iv)** that of the 25 tissues studied only a few selective tissues continued to accumulate aluminum up to 5 months, the longest time-point studied in these experiments, and these include the brain and retina, breast-tissue and ovaries; and **(v)** that aluminum accumulation was directly-associated with up-regulation of the pro-inflammatory transcription factor NF-kB and the inflammatory post-transcriptional epigenetic regulator microRNA-146a in the same tissues. Activation of this aluminum-ROS-NF-kB-miRNA-146a pro-inflammatory genetic circuit is widely observed in AD; and in amyloid- and cytokine-stressed human brain cells in primary culture it marks the onset of neurodegeneration,

neuronal cell dysfunction and apoptotic brain cell death [23,38-42]. Taken together, these results further indicate **(i)** that in aging C57BL/6J murine-models fed aluminum there occurs a selective targeting and accumulation of aluminum in nervous and reproductive tissues which normally exhibit high metabolic rates and high levels in the readout of genetic-information; and **(ii)** that in these same tissues the pro-inflammatory transcription factor NF-kB is significantly up-regulated as is expression of the NF-kB-regulated miRNA-146a, known to be a central driver of pro-inflammatory, innate-immune and pathogenic gene expression programs. Whether aluminum is capable of being 'shuttled' throughout the body mass from one tissue to another, or if there are some synthetic (therapeutic) or natural aluminum removal systems that have evolved to remove this potent neurotoxin from selective physiological compartments are important research questions that remain to be investigated.

Acknowledgments

References

1. Martin RB (1992) Aluminium speciation in biology. Ciba Found Symp 169: 5-18. [View Article]

2. Cuciureanu R, Urzica A, Voitcu M, Antoniu A (2000) A Rev Med Chir Soc Med Nat 104: 107–112.

3. Centers for disease control (CDC) (2012) Atlanta GA, USA, background and environmental exposures to aluminum in the United States. [View Article]

4. Lukiw WJ, Kruck TPA, McLachlan DRC (1989) Aluminium and the nucleus of nerve cells. Lancet 1: 781-782. [View Article]

5. Walton JR, J Alzheimers (2014) Chronic Aluminum Intake Causes Alzheimer's Disease: Applying Sir Austin Bradford Hill's Causality Criteria. J Alzh Dis 40: 765-838. [View Article]

6. Pogue AI, Dua P, Hill JM, Lukiw WJ (2015) Progressive inflammatory pathology in the retina of aluminum-fed 5xFAD transgenic mice. J Inorg Bio 152: 206-209. [View Article]

7. Bhattacharjee S, Zhao Y, Hill JM, Percy ME, Lukiw WJ (2014) Frontiers in Neurology 6: 62-71.

8. Di Paolo C, Reverte I, Colomina MT, Domingo JL, Gómez M (2014) Food Chem Toxicol 69: 320-329.

9. Garcia T, Esparza JL, Nogués MR, Romeu M, Domingo JL, et al. (2010) 20: 218-225.

10. Esparza JL, Garcia T, Gómez M, Nogués MR, Giralt M, et al. (2011) Role of Deferoxamine on Enzymatic Stress Markers in an Animal Model of Alzheimer's Disease After Chronic Aluminum Exposure. Biolog Trace Elem Res141: 232-245. [View Article]

11. Arcía T, Esparza JL, Giralt M, Romeu M, Domingo JL, et al. (2010) Progressive inflammatory pathology in the retina of aluminum-fed 5xFAD transgenic mice. J Inorg Biochem 135: 220-232. [View Article]

12. Drago D, Cavaliere A, Mascetra N, Ciavardelli D, di Ilio C, et al. (2008) Aluminum Modulates Effects of βAmyloid1–42 on Neuronal Calcium Homeostasis and Mitochondria Functioning and Is Altered in a Triple Transgenic Mouse Model of Alzheimer's Disease. Rejuvenation Res11: 861-871. [View Article]

13. Pratico D, Uryu K, Sung S, Tang S, Trojanowski JQ, et al. (2002) FASEB J 16: 1138-1140.

14. Zhang QL, Jia L, Jiao X, Guo WL, Ji JW (2012) Int J Immunopathol Pharmacol 25: 49-58.

15. Oshima E, Ishihara T, Yokota O, Nakashima-Yasuda H, Nagao S, et al. (2013) Accelerated tau aggregation, apoptosis and neurological dysfunction caused by chronic oral administration of aluminum in a mouse model of tauopathies. Brain Pathol 23: 633-644. [View Article]

16. Ribes D, Colomina MT, Vicens P, Domingo JL (2010) Impaired spatial learning and unaltered neurogenesis in a transgenic model of Alzheimer's disease after oral aluminum exposure. Curr Alzheimer Res 7: 401-408. [View Article]

17. Lukiw WJ, Zhao Y, Cui JG (2008) An NF-kappaB-sensitive micro RNA-146a-mediated inflammatory circuit in Alzheimer disease and in stressed human brain cells. J Biol Chem 283: 31315-31322. [View Article]

18. Trapp GA, Miner GD, Zimmerman RL, Mastri AR, Heston LL (1978) Aluminum levels in brain in Alzheimer's disease. Biol Psychiatry 13: 709-718. [View Article].

19. Van der Voet GB, De Hans EJM, De Wolff FA (1985) J Anal Toxicol 9: 97-100.

20. van Ginkel MF, van der Voet GB, de Wolff FA (1990) Improved method of analysis for aluminum in brain tissue. Clin Chem 36: 658-661. [View Article]

21. Pogue AI, Li YY, Cui JG, Zhao Y, Kruck TP, et al. (2009) Characterization of an NF-kappaB-regulated, miRNA-146a-mediated down-regulation of complement factor H (CFH) in metal-sulfate-stressed human brain cells. J Inorg Biochem 103: 1591-1595. [View Article]

22. Li YY, Cui JG, Dua P, Pogue AI, Bhattacharjee S, et al. (2011) Differential expression of miRNA-146a-regulated inflammatory

genes in human primary neural, astroglial and microglial cells. Neurosci Lett 499: 109-113. [View Article]

23. Bhattacharjee S, Zhao Y, Dua P, Rogaev EI, Lukiw WJ (2016) microRNA-34a-Mediated Down-Regulation of the Microglial-Enriched Triggering Receptor and Phagocytosis-Sensor TREM2 in Age-Related Macular Degeneration. PLoS One 11: e0150211. [View Article]

24. Gitelman HJ, Alderman FR (1986) Electrothermal determination of aluminum in biological samples by atomic absorption spectroscopy. Kidney Int Suppl 18: 28-31. [View Article]

25. Qadir MA, Ahmed M, Shahzad S.(2015) Anal Letters 48: 1.

26. Pogue AI, Li YY, Cui JG, Zhao Y, Kruck TP, et al. (2009) Characterization of an NF-kappaB-regulated, miRNA-146a-mediated down-regulation of complement factor H (CFH) in metal-sulfate-stressed human brain cells. J Inorg Biochem 103: 1591-1595. [View Article]

27. Alexandrov PN, Zhao Y, Pogue AI, Tarr MA, Kruck TPA, et al. (2005) Synergistic effects of iron and aluminum on stress-related gene expression in primary human neural cells. J Alzheimer's Dis 8: 117-127. [View Article]

28. Lukiw WJ, Krishnan B, Wong L, Kruck TP, Bergeron C, et al. (1992) Nuclear compartmentalization of aluminum in Alzheimer's disease. Neurobiol of Aging 13: 115-121. [View Article]

29. Bhattacharjee S, Zhao Y, Hill JM, Culicchia F, Kruck TP, et al. (2013) Selective accumulation of aluminum in cerebral arteries in Alzheimer's disease. J Inorg Biochem 126: 35-37. [View Article]

30. Li YY, Cui JG, Hill JM, Bhattacharjee S, Zhao Y, et al. (2011) Increased expression of miRNA-146a in Alzheimer's disease transgenic mouse models. Neurosci Lett 487: 94-98. [View Article]

31. Lukiw WJ, Alexandrov PN, Zhao Y, Hill JM, Bhattacharjee S (2012) Spreading of Alzheimer's disease inflammatory signaling through soluble micro-RNA. Neuroreport 23: 621-626. [View Article]

32. Harvey H, Durant S (2014) The role of glial cells and the complement system in retinal diseases and Alzheimer's disease: common neural degeneration mechanisms. Exp Brain Res 232: 3363-3377. [View Article]

33. Bondy SC (2014) Prolonged exposure to low levels of aluminum leads to changes associated with brain aging and neurodegeneration. Toxicology 315: 1-7. [View Article]

34. Kaur U, Banerjee P, Bir A, Sinha M, Biswas A (2015) Reactive oxygen species, redox signaling and neuroinflammation in Alzheimer's disease: the NF-κB connection. Curr Top Med Chem 15: 446-457. [View Article]

35. Kempuraj D, Thangavel R, Natteru PA, Selvakumar GP, Saeed D, et al. (2016) Neuroinflammation Induces Neurodegeneration. J Neurol Neurosurg Spine 1: 1003. [View Article]

36. Christen Y (2000) Oxidative stress and Alzheimer disease. Am J Clin Nutr 71: 621S-629S. [View Article]

37. Campbell A, Yang EY, Tsai-Turton M, Bondy SC (2002) Pro-inflammatory effects of aluminum in human glioblastoma cells. Brain Res 933: 60-65. [View Article]

38. Griffin WS (2006) Inflammation and neurodegenerative diseases. Am J Clin Nutr 83: 470S-474S. [View Article]

39. Hill JM, Dua P, Clement C, Lukiw WJ (2014) An evaluation of progressive amyloidogenic and pro-inflammatory change in the primary visual cortex and retina in Alzheimer's disease. Front Neurosci 8: 347-352. [View Article]

40. Howlett DR, Attems J, Francis PT (2015) Spreading pathologies precede cognitive decline in Alzheimer's disease. Biol Psychiatry 77: 678-679. [View Article]

41. Walton JR (2013) Aluminum involvement in the progression of Alzheimer's disease. J Alzheimers Dis 35: 7-43. [View Article]

42. Dutescu RM, Li QX, Crowston J, Masters CL, Baird PN (2009) Amyloid precursor protein processing and retinal pathology in mouse models of Alzheimer's disease. Graefes Arch Clin Exp Ophthalmol 247: 1213-1221. [View Article]

43. Golub MS, Donald JM, Gershwin ME, Keen CL (1989) Effects of aluminum ingestion on spontaneous motor activity of mice. Neurotoxicol Teratol 11: 231-235. [View Article]

44. Yuan CY, Lee YJ, Hsu GS (2012) Aluminum overload increases oxidative stress in four functional brain areas of neonatal rats. J Biomed Sci 19: 51. [View Article]

45. Martinez CS, Alterman CD, Pecanha FM, Vassallo DV, Mello-Carpes PB, et al. (2017) Neurotox Res 31: 20-30.

46. Krishnan SS, Gillespie KA, Crapper DR (1972) Determination of aluminum in biological material by atomic absorption spectrophotometry. Anal Chem 44:1469-1470. [View Article]

Supplementary File S1

Determination of aluminum abundance in C57BL/6J mouse tissues using electrothermal atomic-absorption spectrometry (ETAAS)

C57BL/6J mice, sometimes referred to as "C57 black 6", "C57" or "black 6" (standard abbreviation: B6; the second-ever mammalian species to have its entire genome sequenced) is a common inbred strain of laboratory mouse and is currently the most widely used as murine model to study multiple aspects of human disease. C57BL/6J control animals were purchased from a commercial rodent research supplier (http://jaxmice.jax.org/ jaxnotes/507/507r.html; Jackson Laboratories, Bar Harbor MA, USA) and were housed and raised at the LSU animal breeding and holding facility as previously described [6,7]. Altogether 36 female animals per test group (control and aluminum-fed; total N=72 animals) were randomized and selected to receive either standard rodent chow (meal-ground pellets; Standard Laboratory rodent diet 5001; http://www.labdiet.com/cs/groups/ lolweb/@labdiet /documents/webcontent/ mdrf/ mdi4/~edisp/ducm04_028021.pdf ; Lab-Diet St. Louis MO, USA), or a diet enriched in Al (as sulfate; aluminum sulfate is commonly used as food and medicine additive and a water purification agent; http://www.generalchemical.com/assets/ pdf/Dry_Alum_Food_ Grade_PDS.pdf; 100 mg Al/kg diet; LD_{50} for aluminum sulfate in mice ~980 mg Al/kg). Control animals received drinking water containing 0.2 mg/L aluminum (see https://www.wqa.org/Portals/0/ Technical/Technical%20Fact%20Sheets/ 2014 Aluminum.pdf; http://www.who.int/water_sanitation_health/ publications /aluminium/en/) and aluminum-treated animals received aluminum-supplemented water (2.0 mg/L aluminum). The aluminum content of both food and water are physiologically realistic in the consumer environment for daily human exposure; both food and water were provided *ad libitum* from birth. C57BL/6J mice stopped weaning and started eating either standard rodent chow or a diet enriched in Al at about 1 month of age (time '0'); at 0, 1, 3 and 5 months animals were sacrificed, tissues and organs were harvested under RNAse-free clean conditions and were subjected to Zeeman-type ETAAS trace metal analysis for aluminum typically most tissue samples were 0.5 gm wet weight; as required some tissue samples were pooled from several similarly treated animals to achieve enough tissue mass for trace metal analysis.

Murine tissues, chemicals and reagents, protein extraction and quality control

 All analytical and ultrapure chemicals and reagents used in these experiments were obtained from standard commercial suppliers; all chemicals and reagents were used in accordance with the manufacturer's specifications and without any additional purification. Age-matched magnesium sulfate control and aluminum-sulfate-treated C57BL/6J tissues at 0, 1, 3 and 5 months of age were analyzed for aluminum from both control and aluminum-fed animals; total tissue DNA, RNA and protein were isolated using TRIzol reagent as previously described by our group [21-23]; DNA, RNA and protein samples were archived for further downstream and future analysis. For ELISA and Western applications protein concentrations were determined using a dotMETRIC protein microassay as previously described (sensitivity 0.3 ng protein/ml; Invitrogen, Carlsbad, CA, USA; Chemicon-Millipore, Billerica, Massachusetts, USA) [21–31].

Aluminum analysis and ETAAS

Sample Preparation - Individual tissues were dissected free of connective tissue and vasculature and washed in ultrapure water (18 megohm, Millipore or Puriss 95305, Milli-Q water; Fluka; Tracepur® product 1.00473 EMD Merck-Millipore Bellerica MA, USA; aluminum content <1 ppb); samples were next 'dry' ashed in platinum mini-crucibles, taken up in concentrated ultrapure HNO_3 (OmniTrace UltraTM Nitric acid NX0408, EMD Merck-Millipore,

or ULTREX II Ultrapure Reagent, JT Baker/VWR Radnor PA, USA; aluminum content ~20 ppt) and subjected to ETAAS as previously described by our laboratory and others [18-31]. Parallel sets of samples were also analyzed using the 'wet'-digestion method of Trap et al (1978) and Van der Voet (1985) as modified by van Ginkel et al., (1990) [18-20]. In the later method 0.5 gm samples of tissue in disposable polypropylene or Teflon tubes were incubated 24 hr at 45ºC in 0.8 mL concentrated ultrapure nitric acid and 0.2 ml concentrated ultrapure sulfuric acid (ULTREX II Ultrapure Reagent, J.T.Baker/ VWR Radnor PA, USA; aluminum content <50 ppt) in a dedicated 24 position thermomixer/extractor device (Eppendorf model 5436; Eppendorf Inc, Hauppauge NY, USA) with constant agitation; the temperature was next raised to 70ºC for 3 hrs and then 105ºC resulting in a clear yellow solution, diluted up to 3.0 ml with ultrapure water and subjected to trace metal analysis. The use of a dedicated thermomixer device with constant agitation at elevated temperature ensured a thorough concentrated acid-based dissolution of the sample (as suggested by the manufacturer of OmniTrace UltraTM acids; such as Nitric acid NX0408, EMD Merck-Millipore). All sample tubes were spun briefly in a table top microfuge to make sure all liquid in the vial was drained from the seal and the sides of the walls of the analytical tubes prior to analysis.

Analytical Parameters, controls and independent analysis - trace metal analysis was performed in duplicate or triplicate on 20 uL samples using electrothermal atomic absorption spectrophotometry (ETAAS); PE5000PC system, Zeeman-type, Perkin-Elmer, Waltham MA, USA) equipped with an PE automated sampler (18 and 24 position; aluminum detection limit ~2.2 ng/mL) and an IBM/AT-supported analysis package for trace metal analysis, as previously described by our group and others [19-22;26-31]. For multiple sample analyses data were obtained as 'relative signal strength' of aluminum abundance to a standard, or aluminum expressed as ng/gm wet weight of tissue. The ETAAS device hollow-cathode lamp was operated at 15 mA; atomic absorption for aluminum was measured at 309.3 nm with a spectral band width of 0.7 nm; the purge gas was Argon at 300 ml/min gas flow; gas flow was interrupted at atomization; typically the dry cycle was 130ºC, 10 sec ramp, 5 sec hold; char cycle 1500ºC, 18 sec ramp with a 6 sec hold; the atomize cycle was 2700ºC with a 0 sec ramp and a 6 sec hold, although other programs were used with quantitatively similar results; aluminum concentrations in the digest were determined using the standard-addition method. In the later a 10 mg/L aluminum aqueous solution was prepared from ultrapure reagents; aqueous standard solutions of 0, 10, 20 and 50 ug/L were prepared; typically a 250 uL sample of digest was mixed with an equal volume of standard solution prior to analysis in duplicate; the detection limit of this assay was about 5.0 ng aluminum/gm wet weight of tissue [19-23; S Karlik, TPA Kruck, G. Van der Voet, P. Zatta, personal communications). Random murine tissue samples were checked for aluminum content and confirmed independently using an ETAAS device (Perkin-Elmer, Waltham MA, USA) at the Medical Sciences Building, University of Toronto; importantly both the 'dry'- and 'wet' methods of sample preparation gave quantitatively similar results. Some samples were also analyzed at the Advanced Photon Source (APS) using X-ray fluorescence (XRF) spectroscopy with similar results and patterns of murine tissue accumulation of aluminum. In our experiments tissue values ranged from about 25-450 ng/gm wet weight of tissue (**Figure 1**); while tissue accumulation of ingested aluminum appears to be a species-specific phenomenon, the values we obtained in our experiments are in line with other independent laboratory results in rodents [43,44].

ELISA analysis for the NF-kB (p65) subunit

 ELISA analysis for the pro-inflammatory NF-kB transcription factor' were performed using an NF-kB p65 polyclonal antibody [PA1-186; Invitrogen-ThermoFisher Scientific, Waltham MA, USA] and a control protein marker β-actin (3598–100; Sigma-Aldrich Chemical

Company, St. Louis, Missouri, USA) using methodologies previously described by our laboratory and others [17,21,23]. Abundance of the NF-kB (p65) subunit in aluminum-treated versus control samples for 25 murine tissues is shown in bar graph format in **Figure 2**.

Statistical analysis, data interpretation and integrated bioinformatics analysis

For ETAAS data and DNA array analysis all statistical procedures were analyzed using (p, ANOVA) a two-way factorial analysis of variance using algorithms and procedures in the SAS language (Statistical Analysis Institute, Cary, NC, USA) and as previously described [21-23; 26-31]. In the results p-values of less than 0.05 (ANOVA) were considered to be statistically significant. All aluminum, NF-kB and miRNA-146a data were collected and analyzed using Excel 2016 (Office 365) algorithms (Microsoft Corporation, Redmond WA, USA); all figures were generated using Adobe Illustrator CC 2015 and Photoshop CC version14.0 (Adobe Corporation, San Jose CA, USA). All statistical procedures for ELISA were similarly analyzed using a two-way factorial analysis of variance (p, ANOVA) using algorithms, programs and procedures in the SAS language (Statistical Analysis Institute, Cary, NC, USA) and as previously described [29–31]. As before only *p-values* of less than 0.05 (ANOVA) were considered to be statistically significant. Figures were generated using Excel 2008 (Microsoft Corporation, Redmond WA), Adobe Illustrator CS3 ver 11.0 and Photoshop CS2 ver 9.0.2 (Adobe, San Jose CA, USA).